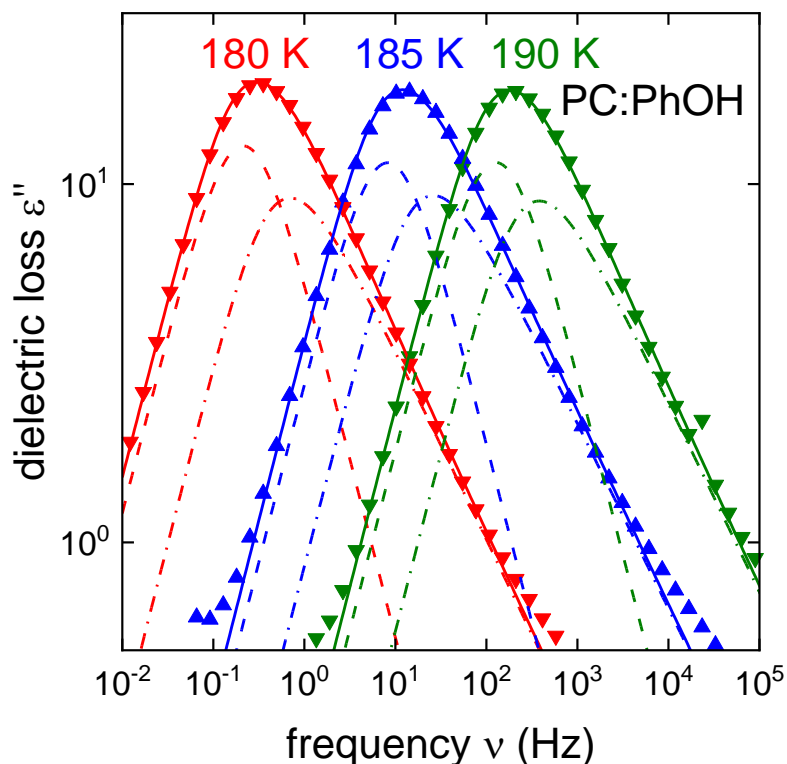# Phenol, the simplest aromatic monohydroxy alcohol, displays a faint Debye-like process when mixed with a nonassociating liquid

Electronic Supplementary Information

Lars Hoffmann, Joachim Beerwerth, Kevin Moch and Roland Böhmer

Fakultät Physik, Technische Universität Dortmund, 44221 Dortmund, Germany

Figure S1: Dielectric loss spectra measured for PC:PhOH. The experimental data (symbols) are decomposed into a Debye-like peak ($\gamma_{CD,D} = 1$), represented by the dashed lines, and an α-type contribution ($\gamma_{CD,\alpha} \approx 0.5$), marked by the dash-dotted lines. The solid lines which illustrate the sum of the two processes describe the experimental data well. The decomposition referring to 180 K is shown also in Figure 2 of the main article.
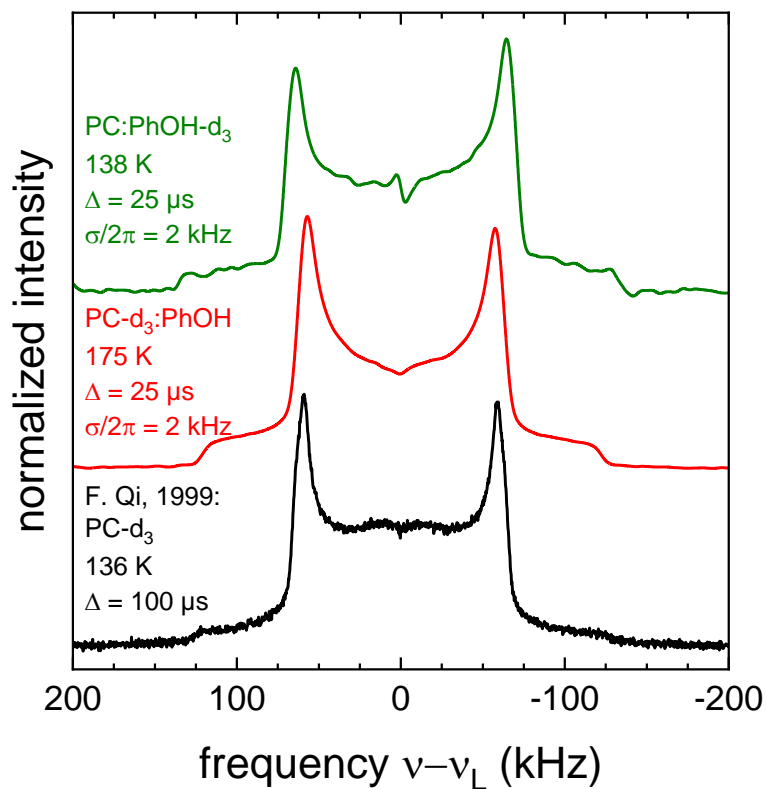
Figure S2: Comparison of low-temperature deuteron solid-echo spectra measured for PC:PhOH-d_3, PC-d_3:PhOH, and PC-d_3.[S1] All spectra are normalized to their peak intensity. The spectral separation of the outer edge singularities is given by $2\delta_Q$ with $\delta_Q = 3e^2qQ / (4h)$ and the asymmetry parameter η can be inferred from the separation $\Delta\nu = (1 - \eta_Q)\delta_Q$ of the horns.[S2] The pulse separation Δ and the Gaussian apodization $\sigma/2\pi$ used for each spectrum is given in the figure.
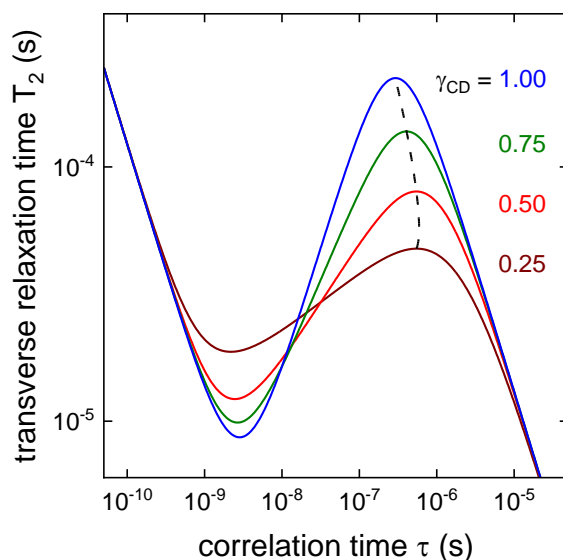
Figure S3: Transverse dephasing times involving contributions from first-and second order quadrupolar relaxation for different Cole-Davidson parameters γ_{CD}. The solid lines are calculated using eqns (13) and (14) of the manuscript for $\omega_0 = 2\pi \times 54.2$ MHz, $C_Q = 8.6$ MHz, and $\eta_0 = 0.7$. The dashed line highlights the shift of the T_2 maximum when varying the Cole-Davidson parameter.
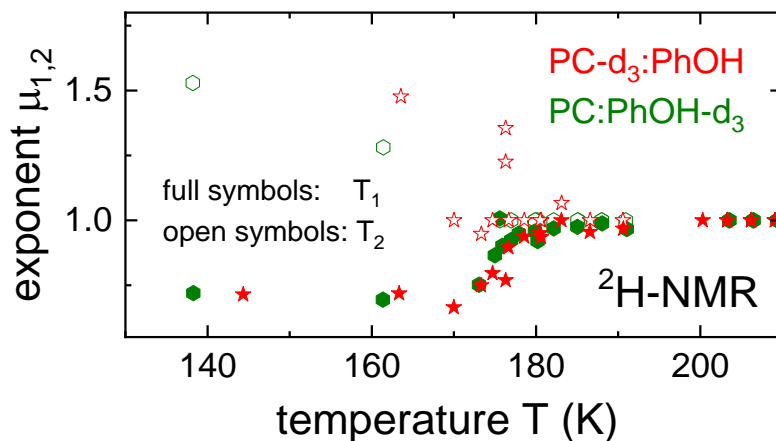
Figure S4: Kohlrausch exponents μ_1 and μ_2 describing the measured deuteron magnetization curves. Above $T = 200$ K the parameters are set to $\mu_1 = \mu_2 = 1$. The observed low-temperature effects are similar to those seen for ^{17}O NMR in the inset of Figure 5. Significant deviations of the deuteron exponents from 1 are only seen below 175 K, while the oxygen magnetization turns nonexponential already below 200 K. This difference can be rationalized by noting that because $T_{1H} \gg T_{1O}$, ergodicity can be restored when τ is longer (before it crosses T_1).

Table S1: Vogel-Fulcher parameters used to calculate the solid lines in the Arrhenius plot (Figure 11) and for the presentation of the computed spin relaxation times (taking into account also the quadrupolar couplings, asymmetry parameters, and Cole-Davidson parameters) in Figure 6. The entries in the second line provides the Vogel-Fulcher data for the the time scales from stimulated echo experiments with an evolution time of 5 μs combined with the correlation times derived from the longitudinal relaxation times. Note that the Vogel-Fulcher parameters in the last line are given already in the main text. Here, they are reproduced to facilitate a comparison with the parameters describing the NMR data.

	T_0	B	$\log_{10}(\tau_0 /s)$	used for Figure	described quantity
PC-d$_3$:PhOH	156 ± 2 K	680 ± 20 K	-12.9 ± 0.3	6, 11	T_1, T_2 and τ determined thereof
PC-d$_3$:PhOH	150 ± 1 K	800 ± 20 K	-13.2 ± 0.1	11	τ_{T1} and τ_{STE}
PC:PhOH-d$_3$	160 ± 2 K	620 ± 25 K	-12.5 ± 0.3	6, 11	T_1, T_2 and τ determined thereof
PC:Ph^{17}OH	161 ± 3 K	610 ± 25 K	-12.3 ± 1.0	5, 6, 11	T_1, T_2 and τ determined thereof
PC:PhOH	140 ± 3 K	1300 ± 100 K	-13.2 ± 0.4	11	τ_{diel} (dominant relaxation)

Details regarding the density functional calculations

Below, the lattice parameters, cell angles, and cell volumes that were experimentally obtained using X-ray diffraction (XRD) at ambient pressure [S3,S4,S5] and at 0.16 GPa[S6] are compared with the CASTEP calculations from ref. [S6] and with those from the present work.

For $p = 0$, after in the present work we performed a geometry optimization, the energy per atom was converged to better than 7×10^{-7} eV, the forces to below 2.1×10^{-2} eV/Å, and the positions to below 1×10^{-3} Å. The structural data from the XRD experiments at $T > 0$ indicate cell constants larger than those that we obtained after geometry optimization. Note that our calculations basically correspond to zero temperature.

For $p = 0.16$ GPa the energy per atom converged to better than 4.2×10^{-6} eV, the forces to below 2.0×10^{-2} eV/Å, and the positions to below 1×10^{-3} Å; furthermore, the maximum stress component was below 47 MPa.

Ambient-pressure phase

a (Å)	b (Å)	c (Å)	γ (°)	V (Å³)	method	reference
5.961	8.878	14.392	90.169	761.60	CASTEP	this work
6.050(1)	8.925(2)	14.594(3)	90.36(2)	788.0(3)	XRD at 123 K	S5
5.97	9.00	15.10	90.0	811.3	XRD at 262 K	S3
6.02	9.04	15.18	90	826	XRD at ambient temperature	S4
6.236	9.071	14.756	90.136	834.70	CASTEP	S6

High-pressure phase

a (Å)	b (Å)	c (Å)	β (°)	V (Å³)	method	reference
11.213	5.322	12.185	102.057	711.11	CASTEP	this work
11.610(4)	5.4416(11)	12.217(5)	101.47(3)	756.4(4)	XRD at 293 K	S6
11.728	5.560	12.332	100.496	790.69	CASTEP	S6

For the ambient pressure phase, the accuracy of the present electrical field gradient parameters C_Q and η (obtained after geometry optimization) were checked by comparison with the data from Ref. [S7]. Those calculations were reported with reference to the crystallographic data from Ref. [S3]. Upon compression the quadrupolar coupling constants (averaged over all lattice sites) obviously change by about 10%.

pressure	0 GPa		0 GPa		0.16 GPa	
Site	C_Q (MHz)	η	C_Q (MHz)	η	C_Q (MHz)	η
O(1)	–8.691	0.85	–8.624	0.79	–8.979	0.967
O(2)	–8.661	0.83	–8.667	0.82	–9.009	0.965
O(3)	–8.706	0.83	–8.705	0.85	–9.012	0.959
average	–8.686	0.84	–8.665	0.82	–9.000	0.959
reference	S7		this work		this work	

References

[S1] Fei Qi, Diploma Thesis, Johannes Gutenberg-Universität, Mainz, 1999; F. Qi, K. U. Schug, S. Dupont, A. Döß, R. Böhmer and H. Sillescu, Structural relaxation of the fragile glass-former propylene carbonate studied by nuclear magnetic resonance, *J. Chem. Phys.*, 2000, **112**, 9455.

[S2] U. Haeberlen, High Resolution NMR in Solids: Selective Averaging, *Advances in Magnetic Resonance*, Academic Press, New York, 1976.

[S3] C. Scheringer, Die Kristallstruktur des Phenols, *Z. Kristallogr.*, 1963, **119**, 273.

[S4] H. Gillier-Pandraud, Structure cristalline du phenol, *Bull. Soc. Chim.*, 1967, **6,** 1988.

[S5] V. E. Zavodnik, V. K. Bel'skii and P. M. Zorkii, Crystal structure of phenol at 123 °K, *J. Struct. Chem.*, 1988, **28**, 793.

[S6] D. R. Allan, S. J. Clark, A. Dawson, P. A. McGregor and S. Parsons, Pressure-induced polymorphism in phenol, *Acta Cryst. B*, 2002, **58**, 1018.

[S7] V. K. Michaelis, B. Corzilius, A. A. Smith and R. G. Griffin, Dynamic nuclear polarization of ¹⁷O: Direct polarization, *J. Phys. Chem. B*, 2013, **117**, 14894.